1   **Highly Active Platinum Single-Atom Catalyst Grafted onto 3D Carbon Cloth Support**

2   **for the Electrocatalytic Hydrogen Evolution Reaction**

3

4   Po-Wei Yu[1], Sait Elmas[1]*, Xun Pan[1], Yanting Yin[1], Christopher T. Gibson[1,2], Gunther G. Andersson[1]
5   and Mats R. Andersson[1]*

6

7   *[1] - Flinders Institute for Nanoscale Science & Technology, Flinders University, Bedford Park SA, Adelaide,*

8   *Australia.*

9   *2 - Flinders Microscopy and Microanalysis, College of Science and Engineering, Flinders University, Bedford*

10   *Park, SA 5042, Australia*

11

12   * - Corresponding authors:
13   Sait Elmas: sait.elmas@flinders.edu.au;
14   Mats Andersson: mats.andersson@flinders.edu.au

15

16   **ABSTRACT**

17   Platinum single-atom catalysts (PtSACs) on 3D support are emerging as new frontier in catalysis due

18   to their atom-economy, outstanding performance and the advantage to bridge the gap between

19   homogeneous and heterogeneous catalysis. Here we report on a simple, single-step electrochemical

20   grafting attachment of a metal-selective ligand, 2,6:2',2"-terpyridine, and the synthesis of platinum

21   single-atom electrocatalyst *via* metal uptake from aqueous salt solution. At an ultra-low loading of

22   0.26 ± 0.02 $\mu g \cdot cm^{-2}$ of platinum, the single atom catalysts supported on porous 3D carbon cloth

23   electrode *via* chemical bonding revealed the highest reported mass activity of 77.1 $A \cdot g_{Pt}^{-1}$ at $\eta = 50$

24   mV/RHE compared to the commercial catalyst 20 % Pt/C. The electro-grafted terpyridine ligand can

25   also act as an effective scavenger for leached platinum from the counter electrode during extended

26   operational hours. The method to make the PtSAC is facile, non-hazardous and versatile without

27   involving any elaborative pre- and/or post-treatment steps and, the value of the added platinum to the

28   ligand is only 0.1 $US\$ \cdot m^{-2}$.

INTRODUCTION

Hydrogen is considered the most promising and competitive energy carrier, as it is clean, renewable and available in abundance. With an energy density of 120-140 MJ/kg being three times higher than the same amount of energy gasoline can provide and the possibility to feed hydrogen gas into the existing infrastructures, the transition from fossil based fuels to the hydrogen economy has started.[1,2] Undoubtedly, when combined with renewable energy sources such as wind and solar power, hydrogen has enormous potential to become one of the main alternative energy carrier to push toward zero greenhouse gas emissions in the near future.[3–5] At present, steam reforming of methanol and ethanol is the main process in hydrogen production. However, the product of the steam reforming is not only hydrogen and water; leaving inevitably the carbon dioxide footprint behind, the question remains as to whether steam-reforming of hydrocarbons can still be defined as "clean". Moreover, the steam reforming process requires high temperature and separation methods making hydrogen as energy carrier also less profitable.[6–8] In contrast, hydrogen production by means of electrocatalytic water splitting is a completely clean method with lower costs and profitable oxygen by-product, which has great potential to produce molecular hydrogen on large scales.[9,10] In electrocatalytic water splitting, platinum based catalysts are used both as cathode and anode due to the high activity of the platinum metal at low overpotentials.[11–13] With its scarcity in the earth's crust (less than 1 $\mu g \cdot kg^{-1}$ availability) and the indispensable applications in catalysis, electronics, jewellery and anti-cancer drugs platinum has inevitably become the most expensive and strategic commodity for the industry nations.[14] Hence, to meet the growing demand and to create higher commercial value, it is of great importance to make every single atom count in electrocatalysis.

54   Recently, the use of single-atom catalysts on solid supports have emerged as new frontier in

55   electrocatalysis due to the atom-economy, where every single atom is involved in the catalytic

56   process. Single-atom catalysts embedded in rationally designed coordination environments and

57   immobilized on stable supports provide the unique advantage to bridge the gap between homogenous

58   and heterogeneous catalysis and keeping the amount of scarce metals at minimum. The synthetic tools

59   to make such single atoms catalysts using Pt include multi-stage wet-chemical synthesis,[15–18] atomic

60   layer deposition,[12,19,20] electrochemical deposition[21–23] and other elaborative methods.[24]

61   A more elegant method to provide a well-defined coordination environment for stable single-

62   atom catalysts is the electrochemical grafting method. In attaching diazonium-substituted ligands onto

63   graphitic and metallic surfaces via strong co-valent chemical bond the grafting method has proven as

64   a powerful tool to address interfacial chemistry.[22,25–27]

65   Herein, we report on a simple single-step-electrochemical grafting technique to make stable

66   Pt single-atom catalysts (PtSAC) embedded in a strong coordination environmental for platinum

67   group metals. The coordination environment is provided by the 2,6:2',2"-terpyridine pincer type

68   ligand[28–30] that allows tailored mass loading by uptake of Pt^{2+} from commercially available platinum

69   salts in aqueous solution. Furthermore, the electro-grafted terpyridine ligand on the 3-dimensional

70   carbon cloth electrode serves as highly efficient metal scavenger for recovering leached platinum

71   from the counter electrode (Fig. 1). Platinum leaching from the counter electrodes during long-term

72   operation in acidic media has been in focus of recent studies questioning the reliability of Pt as

73   counter electrode in membrane-less electrolysers.[31–35] Significant loss of the noble metal stemming

74   from the counter electrode is observed in the electrolyte.[33,36] In this study, leached platinum atoms are

75   scavenged by the terpyridine ligand and utilized *in-situ* as additional single-atom catalysts improving

76   the catalysts performance as the hydrogen evolution reaction progresses.

77
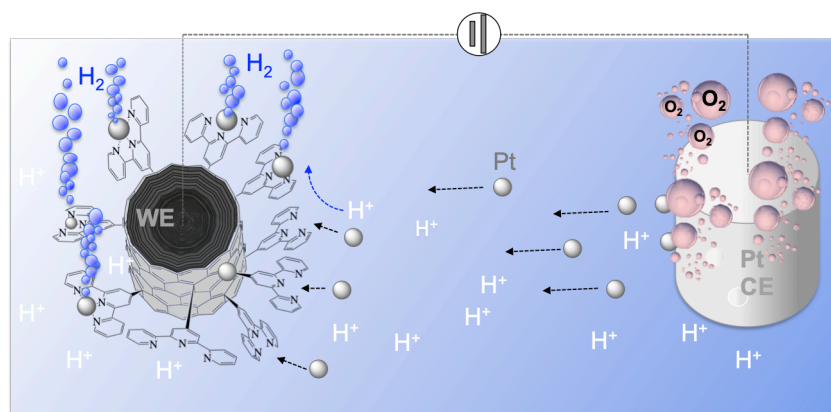
Figure 1: Hydrogen production on Pt single atoms embedded in terpyridine coordination environment electro-grafted onto the carbon cloth (WE) fibre. The electro-grafted ligand acts also as vacancy for leached Pt ions from the counter electrode (CE).

The preparation of the electrocatalyst from commercially available products is non-hazardous, versatile and does not require any elaborative and expensive pre- and/or post-treatment. To the best of our knowledge, this is first report on single-step electro-grafting method to chemically bind 2,6:2',2"-terpyridine directly onto 3D carbon support and fabrication of single-atom catalysts by simple metal uptake from commercially available metal salts.

EXPERIMENTAL

Materials and methods. Sulfuric acid (98%, Scharlau), hydrochloric acid (Sigma Aldrich, analytical grade) and potassium hydroxide (Scharlau, Spain) were diluted with MilliQ water (TOC 1.8 ppm, 18.2 ΩMcm@25°C) to the required molarities in 100 mL volumetric flasks. Sodium nitride, $NaNO_2$, and potassium tetrachloroplatinate, $K_2[PtCl_4]$, were purchased from Sigma Aldrich and used without further purification. 4'-Amino-2,2':6',2'-terpyridine was purchased from Shanghai UCHEM Inc. (Shanghai, China) and used without further purification.

97   Carbon cloth (Plain Carbon Cloth 1071, SKU 591342-1) and 0.03 mg/cm² 20% Platinum on

98   Vulcan – Cloth (W1S1009) were purchased from FuelCellStore (Fuel Cell Etc, USA) and cut into 1 x

99   5 cm^2 pieces to obtain the carbon cloth (CC) and 20% 0.03 mg Pt/C electrodes.

100   XPS was applied using Mg Kα radiation to determine the elemental composition and the chemical

101   states of all components. Under the condition chosen, XPS has a probing depth of less than 10 nm,

102   depending on the electron mean free path.[37] The apparatus was built by SPECS (Berlin, Germany)

103   with a non-monochromatic X-ray source and has and a base pressure of a few 10^{-10} mbar with the

104   details described in.[38] The angle between the X-ray source and the analyser is 54.7 °. At a pass energy

105   of 10 eV the FWHM of the Ag $3d_{5/2}$ peak is < 1 eV. The uncertainty of the peak positions is typically

106   0.2 eV. High-resolution scans were recorded at a step size of 0.1 eV for C, O, N and Pt at a pass

107   energy of 10 eV. The acquired spectra were calibrated by setting the C 1s peak of C-C sp^3 carbon to

108   285.0 eV.

109   Data analysis was performed with CasaXPS software (Casa Software Ltd.) and selected graphs were

110   plotted with the Qti Plot software.

111   Raman spectra were acquired using a Witec alpha300R Raman microscope at an excitation

112   laser wavelength of 532 nm with a 40X objective (numerical aperture 0.60). Typical integration times

113   for single Raman spectra were 5 to 15 s and averaged from 2 to 3 repetitions. 10 to 15 spectra were

114   acquired per sample with spectra analysed using Witec project 4.1.

115   Thermogravimetric analysis (TGA) measurements were performed on PerkinElmer TGA

116   8000, with the temperature range of 30 - 1000 °C under nitrogen gas protection, and the heating ramp

117   of 10 °C•min^{-1}. All samples were dried in a vacuum oven at RT prior to the measurements.

118   Electrochemical data were recorded on an AUTOLAB potentiostat (Metrohm, Switzerland) in

119   0.5 M HCl for the electro-grafting step and 0.5 M H_2SO_4 for electrocatalytic studies using modified

120   carbon cloth as working electrode (WE), a platinum wire or graphite rod as counter electrode (CE)

121   and Ag|AgCl (1M KCl) as reference electrode. Recorded potentials were converted into reversible

122   hydrogen electrode (RHE) as reported elsewhere.[39]

123   Inductively coupled plasma optical emission spectroscopy (ICP-OES) was conducted on a

124   Perkin Elmer Optima 800 instrument using standard calibration between 10 and 500 ppb Pt^{2+}.

125   ***Electro-grafting of the terpyridine ligand onto the plain CC electrode, terpy@CC.*** In a 20

126   mL electrochemical cell, 16.8 mg (0.068 mmol) of 4'-amino-2,2':6',2''-terpyridine and 37.4 mg (0.44

127   mmol) of sodium nitrate were dissolved in 10 mL of 0.5 M HCl solution and purged with N_2 for 15

128   minutes. Then, 10 consecutive cyclic voltammetry scans were applied at 10 mVs^{-1} between 0.2 and -

129   1.0 volts using the plain carbon cloth (1 x 5 cm) as working, Pt wire as counter and Ag|AgCl (1M

130   KCl) as reference electrode. After the grafting step was finished, the submerged (grafted) surface area

131   of CC was measured and the obtained Terpy@CC electrode was stored in a 0.1 M KOH solution for

132   at least 30 minutes, then washed with MilliQ water, then EtOH and dried in the vacuum oven

133   overnight.

134   ***Pt^{2+} uptake by the terpy@CC electrode.*** The terpy@CC electrodes were cut to small pieces

135   (typically 2 cm x 1 cm) and submerged in dark inside a closed vial containing 20 mL aqueous

136          $K_2[PtCl_4]$ solution with an available concentration of 0.5 ppm Pt^{2+} for 2 h at room temperature (RT).

137   The MilliQ water was purged for at least 30 min with N_2 prior to dissolving the platinum salt. After 2

138   h uptake, the closed vial was gently shaken and 18 mL of the Pt^{2+} solution was analysed by ICP OES.

139   To validate the Pt^{2+} uptake by terpy@CC, two control experiments were conducted with pure CC

140   electrodes and no absorbent added to the 0.5 ppm Pt^{2+}. In total, four uptake experiments were

141   conducted, and the remaining Pt^{2+} solutions after uptake were analysed by ICP OES. Whereas no

142   concentration difference between both control samples was detected by ICP OES, the concentration

143   difference after uptake by the terpy@CC electrode was calculated to be 0.26 ± 0.02 μg·cm^{-2}.

144

145   **RESULTS AND DISCUSSION**

146   ***Synthesis and performance of the Pt single-atom catalysts in HER***

147   Terpyridine is a versatile ligand in coordination chemistry, it is well-known for its strong

148   binding character to noble metals and has a widespread applications in molecular architectures.[40–45]

149 The plain carbon cloth (CC) has high electrical conductivity and is an ideal support material for self-

150 supported electrocatalysts.[46,47] The flexible 3-dimensional woven structure that provides relatively

151 large specific surface area can accommodate a high number of grafted ligands via covalent bonds,

152 enabling the combination of single-atom chemistry with 3D supported catalysis. To make the stable 3-

153 dimenisional and metal-chelating electrode, the terpyridine ligand was electro-grafted onto the carbon

154 cloth electrode under cathodic reduction in 0.5 M HCl solution using cyclic voltammetry. 4-

155 Diazonium-2,2':6,2"-terpyridine was generated *in-situ* with sodium nitrite in 0.5 M HCl and subjected

156 to electrochemical grafting (see Experimental and Scheme 1a).[27,48,49] As shown in Fig 2a, a strong

157 reduction event appears at -0.68 V vs. RHE during cathodic cycling in 0.5 M HCl electrolyte solution.

158 The strong reduction event originates from the homolytic cleavage of $C-N_2^+$ bond creating a

159 terpyridine radical that immediately reacts with the carbon surface (Scheme 1b). Within the

160 subsequent numbers of cathodic sweeps, the intensity of observed reduction peak decreases rapidly, a

161 typical indication for surface saturation with electro-grafted ligands.[50,51] The rapid decrease in the

162 reduction peak and the absence of additional reduction events during progressing cyclic voltammetry

163 sweeps is indicative for single layer grafted terpyridine ligands. Note that, from one single ligand

164 solution a series of terpyridine-grafted CC electrodes could be prepared highlighting the advantage of

165 the electrochemical grafting method. Thermogravimetric analysis shows the ligand being stable on the

166 carbon cloth surface up to 300°C (terpy@CC, Fig. 2b) and XPS surface analysis of the electro-grafted

167 carbon cloth electrode detected high content (up to 10%) of nitrogen on the surface, which is

168 attributed to the ligand (vide infra).

7

(a)

(b)

PtSAC@CC

169
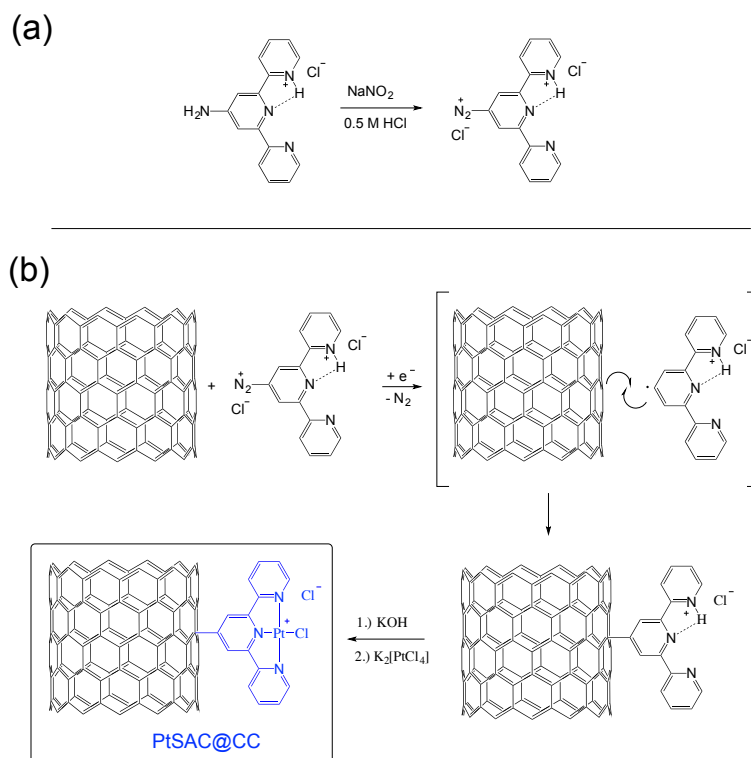
170 **Scheme 1**: **(a)** *In-situ* preparation of 4-diazonium 2,2':6,2"-terpyridine in 0.5 M HCl electrolyte solution using

171 sodium nitrite as oxidant and, **(b)** subsequent electrochemical grafting of the terpyridine ligand onto the 3-

172 dimenisonal carbon cloth at -0.68 V vs. RHE. The synthesis of the platinum single-atom electrocatalyst, PtSAC,

173 is achieved by metal uptake from aqueous $K_2[PtCl_4]$ solution.

174

175   To make the single-atom Pt electrocatalyst (PtSAC@CC-0.5), the terpy-grafted CC electrode,

176 terpy@CC, was submerged in aqueous potassium tetrachloroplatinate solution (0.5 ppm Pt^{2+}) for 2 h

177 at RT. In our studies, we found that increased temperature, exposure to light and presence of

178 dissolved oxygen caused formation of Pt deposition on the non-grafted CC electrode itself. Hence, to

179 avoid deposition of nano-particulate platinum on the CC surface, the Pt^{+2} uptake was conducted under

180 N_2 protection and in the dark. Under these conditions, repeated uptake experiments from 0.5 ppm Pt^{2+}

181 ions revealed mass loadings of 0.26 ± 0.02 µg·cm^{-2} of platinum on the terpy@CC electrodes,

182 whereas no Pt uptake from pure CC could be detected by ICP OES.
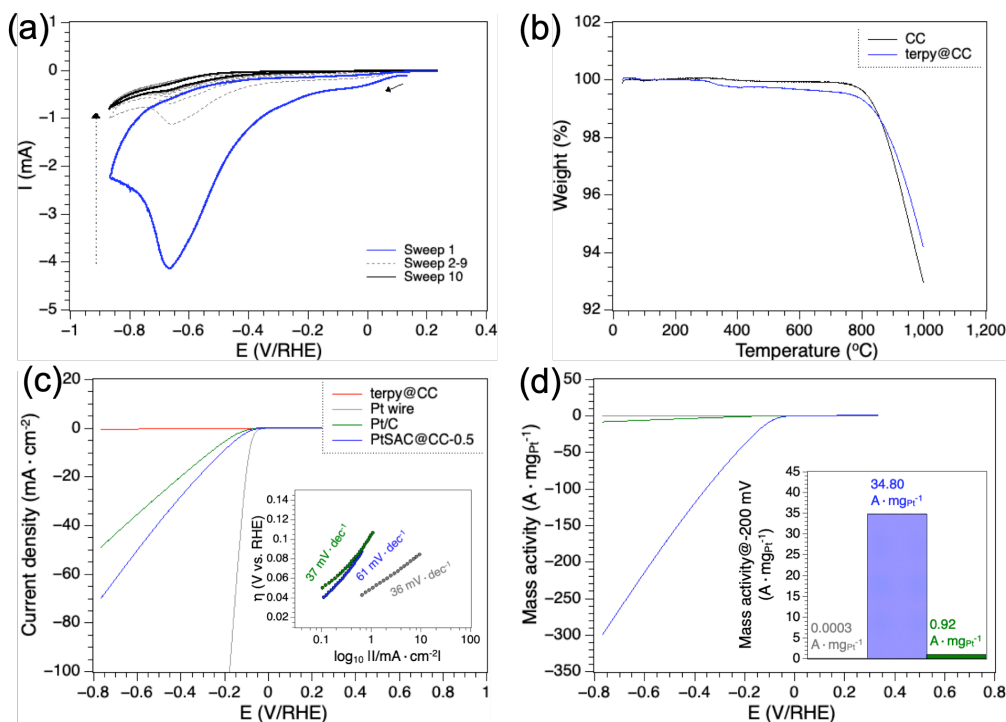
Figure 2: Recorded cyclic voltammogram of electro-grafting 4-amino terpyridine onto the carbon electrode in 0.5 M HCl electrolyte solution. (b) TGA thermogram of the electro-grafted ligand (terpy@CC) compared to the blank support carbon cloth (CC). (c) Linear sweep voltammogram of the Pt single-atom catalyst (PtSAC@CC-0.5) compared to the free ligand terpy@CC (red), commercial catalyst 0.03 mg 20% Pt/C@CC (green) and the Pt wire (grey); inset shows the calculated Tafel slopes with their respective colour scheme. (d) Calculated mass activity of the catalysts as function of applied potential vs. RHE in their respective colour; inset shows comparative mass activity at the overpotential of 200 mV.

The HER activity of the single-atom Pt catalyst, PtSAC@CC-0.5, was studied in 0.5 M H_2SO_4 solution using a Pt wire and Ag|AgCl (1 M KCl) as counter and reference electrode, respectively. For comparisons, commercially available benchmark catalyst on carbon cloth, 20% 0.03 mg Pt/C, a platinum wire and the free ligand electro-grafted onto the CC electrode were tested under the same conditions. For a better accuracy of the performance data and to avoid potential metal leaching from the Pt counter electrode and re-deposition onto the working electrode in acidic media, only 10 cyclic voltammetry sweeps at 10 mV·s^{-1} were applied. Figure 2c shows the last forward

9

199   sweep of the recorded cyclic voltammograms, each. It appears that the single atom catalyst slightly

200   outperforms the commercially available benchmark catalyst, 20% 0.03 mg Pt/C, when normalised to

201   the geometric surface area. To generate 10 mA·cm^{-2}, PtSAC@CC-0.5 requires 210 mV vs. RHE,

202   which is 59 mV lower than Pt/C. The Tafel slopes were calculated in the low overpotential range of

203   40-110 mV to be 61, 37 and 36 mV·dec^{-1} for the PtSAC@CC-0.5, Pt/C and the Pt wire, respectively.

204

205   **Table 1:** Calculated mass activity ratios of the PtSAC and 20% Pt/C studied in this work and compared to the

206   activity ratios of Pt single-atom catalysts reported in literature.

Overpotential	Mass activity ratio between studied catalyst and 20% Pt/C	
η (V/RHE)	This work	Literature
50 mV	77.1	74.4[52], 40[53], 37.4[12], 4.3[13]
100 mV	51.3	47.56[53], 26.9[54], 6.1[13]
200 mV	37.8	6.3[55]

207

208   To compare the activity with reported platinum single-atom catalysts the linear sweep

209   voltammograms in Fig. 2c were converted into the mass activities (Fig. 2d). Here, our PtSAC@CC-

210   0.5 outperforms by far the Pt wire and the commercial catalysts Pt/C making literally every single

211   atom count in the hydrogen evolution reaction. When normalised to the mass loading of Pt/C, the

212   ultra-low loading of 0.26 ± 0.02 µg·cm^{-2} platinum places the single-atom catalyst, PtSAC@CC-0.5

213   in an highly competitive position. As summarized in Table 1, the PtSAC@CC-0.5 self-supported on

214   the 3D carbon cloth electrode is slightly better than the highest reported mass activities at

215   overpotentials of 50, 100 and 200 mV, respectively.

216
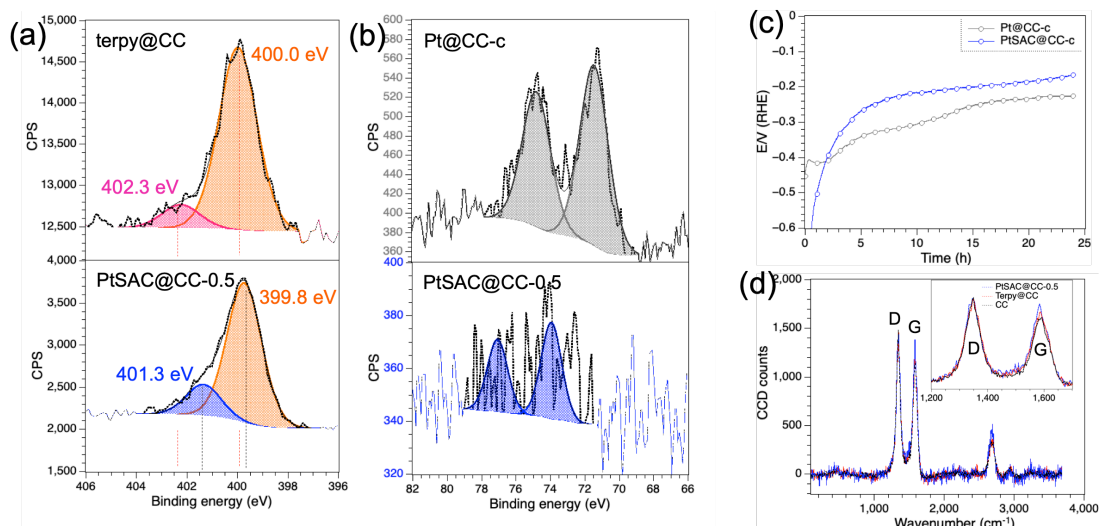
Figure 3: (a) Fitted N1s and (b) Pt4f core level spectra of the electro-grafted terpyridine onto carbon cloth (terpy@CC), ultra-low platinum-loaded single atom catalyst (PtSAC@CC-0.5) and Pt-loaded carbon cloth after 24 h chronoamperometric (Pt@CC-c); the ultra-low loading of the electro-grafted terpy@CC electrode was carried out from 0.5 ppm Pt^{2+} ion solution and the Pt-loading onto CC electrode stems from Pt leaching from the CE and re-deposition onto the WE; (c) Chronoamperometric HER at 10 $mA \cdot cm^{-2}$ for 24 h on PtSAC@CC-0.5 and CC electrode. Due to the Pt leaching and re-deposition onto the working electrodes, both electrodes became PtSAC@CC-c and Pt@CC-c; (d) Overlapped D and G Raman bands of CC, Pt@CC, terpy@CC and PtSAC@CC-0.5.

Surface analysis by X-ray photoelectron spectroscopy (XPS) was carried out to investigate the valence state of the metal in PtSAC@CC-0.5 and to understand the participation of the coordination environment in the electro-grafted terpyridine ligand. The fitted N(1s) and Pt(4f) core level spectra are shown in Fig. 3 and summarized in Table 2. Electro-grafted CC showed under XPS more than 10% nitrogen with the N1s core level spectrum fitted to a main peak at 400 eV accompanied by a peak at 402.3 eV (Fig. 3a). The first peak is assigned to the pyridine structure while the second peak originates from ammonium-N after electro-grafting the ligand under acidic conditions (see mechanism in Scheme 1).[56] After Pt uptake from 0.5 ppm Pt^{2+} ions, both N peaks were shifted toward lower binding energies (BE) where the =N-H$^+$ peak featuring a significant shift to lower

The XPS core level spectra of platinum exhibit two asymmetric components in the Pt4f region (Pt4f$_{5/2}$ and Pt4f$_{7/2}$) and are separated by 3.33 eV as expected for Pt. Leached platinum that only originates from the counter electrode during 24 hours chronoamperometric water splitting and re-deposited onto the WE (Pt@CC-c, Fig. 3b, top panel) exhibits only zero-valent platinum (Pt^0), whereas the terpyridine-grafted electrode pre-loaded with Pt^{2+} ions from 0.5 ppm solution shows trace amounts Pt^{2+} at 73.8 eV as oxide under XPS (see Fig. 3b bottom panel and Table 2).[53,57] The binding energy of the first component is 71.5 eV assigned to metallic Pt.[58] The binding energy of the second component is at 73.9 eV and assigned to Pt^{2+} as part of PtCl$_2$ or PtO bound into the terpyridine units. Although 10 linear sweeps were applied to PtSAC@CC-0.5, XPS analysis of the electrode showed no indication of reduced platinum.

Table 2: Fitted XPS core level data in Pt4f, their atomic composition and ratios as well as the Raman D/G ratios of studied electrodes.

Electrode	% C	% O	% N	% Pt	N/Pt	Pt^0	Pt^{2+}	D/G
CC	95.06	4.94	0	0	-	-	-	1.28
Pt@CC-c	96.15	3.67		0.19	-	71.5		1.14
Terpy@CC	78.41	11.17	10.71	-	-	-	-	1.17
PtSAC@CC-0.5	76.05	11.62	12.27	0.03	409		73.9	1.07
PtSAC@CC-0.5c	72.83	14.38	11.09	1.46	7.6	71.4	73.9	
PtSAC@CC-165	66.85	18.85	9.50	2.81	3.38	72.0	73.7	

After chronoamperometric water splitting at PtSAC-0.5 (Fig. 3c), XPS detected a mixture of zero- and bi-valent platinum on the electrode, where Pt^0 is major valence state (PtSAC@CC-0.5c in Fig. 4b). In stark contrast to the ligand-free CC electrode, much stronger deposition onto the terpy-grafted WE was detected by XPS. The Pt content increased from 0.03% to 1.46% after 24 h operation, whereas the increase of Pt content on ligand-free CC was only by 0.19%. This observation is also indicated by the steep decrease of the overpotential at the PtSAC-0.5c electrode during the

chronoamperometric water splitting (see Fig. 3c) suggesting that leached Pt from the counter

electrode is immediately bound into chelating interface of the working electrode.
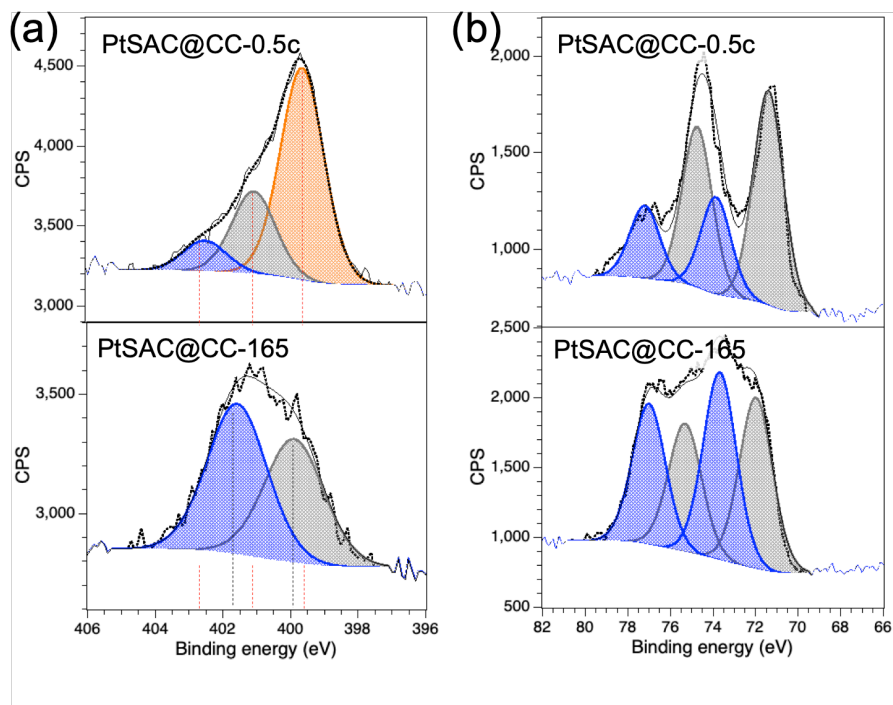
Figure 4: Fitted (a) N1s and (b) Pt4f core level spectra of the ultra-low platinum-loaded single atom catalyst

(PtSAC@CC-0.5c) after 24 h chronoamperometry (top panels) and after uptake of Pt^{2+} from 165 ppm Pt ion

solution (bottom panels).

When using graphite rod as counter electrode in a separate chronoamperometric HER

experiment on PtSAC-0.5, XPS detected Pt^{2+} as only valence state with no loss of metal after 3 h of

operation suggesting that presence of the Pt^0 in the previous experiment (PtSAC-0.5c) was largely

contributed by leached metal from the Pt CE (Fig. S1, Supporting Information). Using again Pt as CE

in further control experiments with 8 hours chronoamperometric HER on the PtSAC@CC-0.5 and CC

electrodes showed 240-260 ppb Pt being leached into the electrolyte solution, when the electrolytes

were analysed by ICP OES. It was also found that re-deposited Pt onto CC in both valence states Pt^0

and Pt^{2+} was removed by more than 71% when the working electrode was sonicated for 40 minutes in

271 pure H_2O and then subjected to surface analysis by XPS (see Fig. 5b). In contrast, bound Pt^{2+} into the

272 terpy@CC electrode was not removed from the chelating pockets after the same time of sonication

273 (Fig. 5a). Again, this method clearly highlights the main advantage of the terpyridine ligand on CC

274 support as it acts as efficient scavenger for leached platinum.

275

276
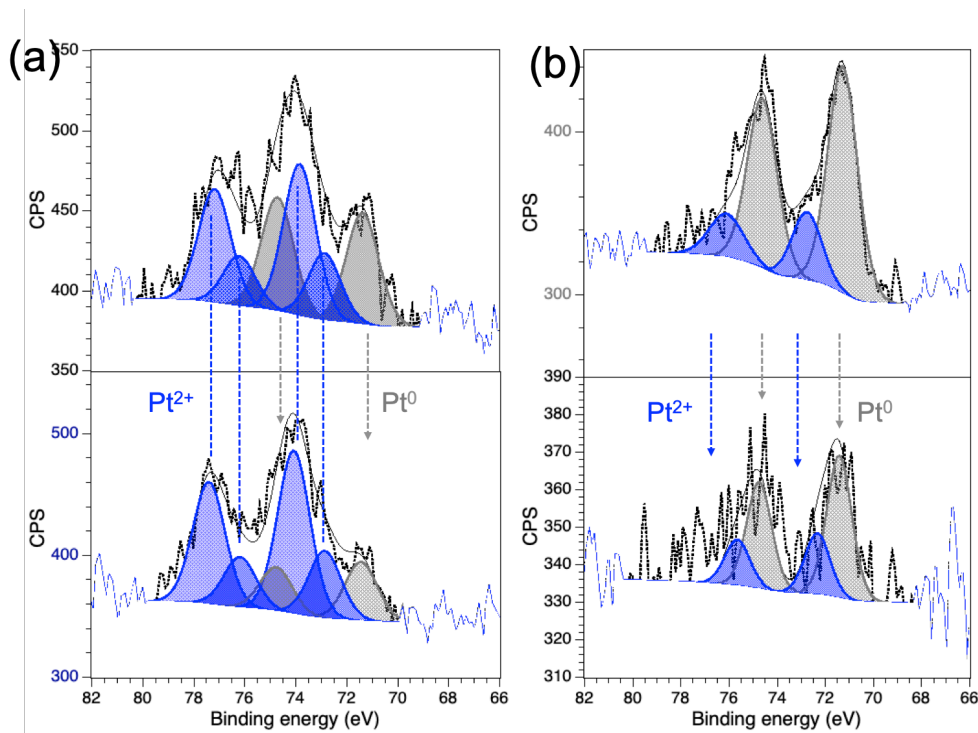
277 **Figure 5:** (a) Fitted Pt4f core level spectra of the ultra-low platinum-loaded single atom catalyst (PtSAC@CC-

278 0.5) after 8 h chronoamperometry (top panels) and after 40 min sonication (bottom panel) using the Pt wire as

279 CE; (b) Fitted Pt4f core level spectra of leached Pt and deposited onto CC after 8 h chronoamperometry (top

280 panels) and after 40 min sonication (bottom panel) using the Pt wire as CE.

281

282 As shown in Fig. 4a (top panel), three components were fitted to the N1s core level spectrum

283 of PtSAC@CC-0.5c, that is assigned to the nitrogen in the free ligand (orange) and the N-donors

284 bound to Pt^0 (grey) and Pt^{2+} (blue), respectively. Although significant amounts of Pt were leached and

285 bound to the terpy@CC interface, only less than a half of the available ligands were occupied by Pt

286 (N/Pt ratio of 7.6 in Table 2). A nearly full saturation with Pt was found in uptake experiments within

287 2 hours, when the concentration of the available Pt ions was increased to 165 ppm (N/Pt ratio of 3.38

288 in PtSAC@CC-165, Table 2). Notably, the fitted components in Pt4f core level data revealed high

289 amounts of zero-valent platinum in PtSAC@CC-165, although the uptake was from Pt^{2+} ions. In line

290 with the reported studies in the literature, it appears to be difficult to obtain either one of the valence

291 Pt^0, Pt^{2+} or Pt^{4+} at higher metal loadings.[59] Of particular note is also the observed I_D/I_G ratio in the

292 Raman spectra (Fig. 3d). The intensity and positions of Raman peaks can provide important

293 structural information for the carbon samples. The G peak between 1560 to 1600 cm^{-1} is

294 associated with a vibrational mode of sp^2-hybridized graphene planes. The D peak at 1300 to

295 1400 cm^{-1} is the band associated with defects. The ratio of D band to G band peak intensities,

296 I_D/I_G, has been used to probe the level of disorder of carbon materials.[52] Non-grafted CC displays

297 the highest ratio between the D- and G-band indicative for highest defects of the carbon surface in this

298 series. As the surface is manipulated further, more symmetry is induced as indicated in the decay of

299 the I_D/I_G ratio that approaches a ratio of 1/1. This tendency has also been observed in similar catalysts

300 systems and explained by coverage of the defects after manipulating the carbon fibre surface (Table

301 2).[52]

302

303

304 **CONCLUSIONS**

305 Functionalisation of the 3D carbon cloth surface with well-defined coordination environment

306 by simple electrochemical grafting methods enables to access ultra-low loaded and high performing

307 single atom catalysts for electrocatalytic applications. In this study, using the terpyridine ligand as

308 strong chelator for noble metals, platinum single-atom catalysts were made in two simple steps

309 without involving elaborative synthetic methods. The obtained PtSAC@CC-0.5 revealed the lowest

310 reported mass loading of 0.26 ± 0.02 µg•cm^{-2} and the highest reported mass activity ratio of 77.1

311 A•g_{Pt}^{-1} at η = 50 mV/RHE in the electrocatalytic hydrogen production compared to the benchmark

312 catalyst Pt/C. This method provides dual benefit for the scarcity of the noble metals. In pushing the Pt

313 value down to 0.1 US\$•m^{-2} compared to 2.30 US\$•m^{-2} for 20% 0.03 mg Pt/C (see Supporting

314 Information) it makes literally every single atom count in electrocatalysis and recovers leached metal

315 from counter electrodes at the same time.

316

326

327 **AUTHORS CONTRIBUTION**

328   P.-W. Y. and S. E. contributed equally.

329

330 **CONFLICT OF INTEREST**

331   The authors declare no conflict of interest.

332

333 **ABBREVIATIONS**

334 CC – Carbon cloth electrode.

335 terpy – Terpyridine ligand

336 terpy@CC – terpyridine ligand electro-grafted onto the CC surface

337 PtSAC – Platinum single-atom catalyst.

338 PtSAC@CC – Platinum single-atom catalyst bound into terpy@CC.

339 PtSAC@CC-0.5 – PtSAC@CC obtained from 0.5 ppm Pt^{2+} solution.

340 PtSAC@CC-0.5c – PtSAC@CC obtained from 0.5 ppm Pt^{2+} solution and after chronoamperometric

341 HER.

342 PtSAC@CC-165 – PtSAC@CC obtained from 165 ppm Pt^{2+} solution.

343 Pt@CC-c – leached platinum from Pt CE and re-deposited onto the CC working electrode after

344 chronoamperometric HER.

345

346 **REFERENCES**

347 (1) Abe, J. O.; Popoola, A. P. I.; Ajenifuja, E.; Popoola, O. M. Hydrogen Energy, Economy
348 and Storage: Review and Recommendation. *International Journal of Hydrogen*
349 *Energy* **2019**, *44* (29), 15072–15086.
350 https://doi.org/10.1016/j.ijhydene.2019.04.068.
351 (2) Pudukudy, M.; Yaakob, Z.; Mohammad, M.; Narayanan, B.; Sopian, K. Renewable
352 Hydrogen Economy in Asia – Opportunities and Challenges: An Overview.
353 *Renewable and Sustainable Energy Reviews* **2014**, *30*, 743–757.
354 https://doi.org/10.1016/j.rser.2013.11.015.
355 (3) Hsu, S.-H.; Miao, J.; Zhang, L.; Gao, J.; Wang, H.; Tao, H.; Hung, S.-F.; Vasileff, A.;
356 Qiao, S. Z.; Liu, B. An Earth-Abundant Catalyst-Based Seawater Photoelectrolysis
357 System with 17.9% Solar-to-Hydrogen Efficiency. *Adv. Mater.* **2018**, *30* (18),
358 1707261. https://doi.org/10.1002/adma.201707261.
359 (4) Lin, L.; Zhou, W.; Gao, R.; Yao, S.; Zhang, X.; Xu, W.; Zheng, S.; Jiang, Z.; Yu, Q.; Li, Y.-
360 W.; Shi, C.; Wen, X.-D.; Ma, D. Low-Temperature Hydrogen Production from Water
361 and Methanol Using Pt/α-MoC Catalysts. *Nature* **2017**, *544* (7648), 80–83.
362 https://doi.org/10.1038/nature21672.
363 (5) Momirlan, M.; Veziroglu, T. N. Current Status of Hydrogen Energy. *Renewable and*
364 *Sustainable Energy Reviews* **2002**, *6* (1–2), 141–179.
365 https://doi.org/10.1016/S1364-0321(02)00004-7.
366 (6) LeValley, T. L.; Richard, A. R.; Fan, M. The Progress in Water Gas Shift and Steam
367 Reforming Hydrogen Production Technologies – A Review. *International Journal*
368 *of Hydrogen Energy* **2014**, *39* (30), 16983–17000.
369 https://doi.org/10.1016/j.ijhydene.2014.08.041.
370 (7) Palo, D. R.; Dagle, R. A.; Holladay, J. D. Methanol Steam Reforming for Hydrogen
371 Production. *Chem. Rev.* **2007**, *107* (10), 3992–4021.
372 https://doi.org/10.1021/cr050198b.

373   (8)   Holladay, J. D.; Hu, J.; King, D. L.; Wang, Y. An Overview of Hydrogen Production
374   Technologies. *Catalysis Today* **2009**, *139* (4), 244–260.
375   https://doi.org/10.1016/j.cattod.2008.08.039.
376   (9)   Nong, H. N.; Gan, L.; Willinger, E.; Teschner, D.; Strasser, P. IrOx Core-Shell
377   Nanocatalysts for Cost- and Energy-Efficient Electrochemical Water Splitting.
378   *Chem. Sci.* **2014**, *5* (8), 2955–2963. https://doi.org/10.1039/C4SC01065E.
379   (10)   You, B.; Sun, Y. Innovative Strategies for Electrocatalytic Water Splitting. *Acc.*
380   *Chem. Res.* **2018**, *51* (7), 1571–1580.
381   https://doi.org/10.1021/acs.accounts.8b00002.
382   (11)   Reier, T.; Oezaslan, M.; Strasser, P. Electrocatalytic Oxygen Evolution Reaction
383   (OER) on Ru, Ir, and Pt Catalysts: A Comparative Study of Nanoparticles and Bulk
384   Materials. *ACS Catal.* **2012**, *2* (8), 1765–1772.
385   https://doi.org/10.1021/cs3003098.
386   (12)   Cheng, N.; Stambula, S.; Wang, D.; Banis, M. N.; Liu, J.; Riese, A.; Xiao, B.; Li, R.;
387   Sham, T.-K.; Liu, L.-M.; Botton, G. A.; Sun, X. Platinum Single-Atom and Cluster
388   Catalysis of the Hydrogen Evolution Reaction. *Nat Commun* **2016**, *7* (1), 13638.
389   https://doi.org/10.1038/ncomms13638.
390   (13)   Cheng, X.; Li, Y.; Zheng, L.; Yan, Y.; Zhang, Y.; Chen, G.; Sun, S.; Zhang, J. Highly
391   Active, Stable Oxidized Platinum Clusters as Electrocatalysts for the Hydrogen
392   Evolution Reaction. *Energy Environ. Sci.* **2017**, *10* (11), 2450–2458.
393   https://doi.org/10.1039/C7EE02537H.
394   (14)   Reith, F.; Campbell, S. G.; Ball, A. S.; Pring, A.; Southam, G. Platinum in Earth
395   Surface Environments. *Earth-Science Reviews* **2014**, *131*, 1–21.
396   https://doi.org/10.1016/j.earscirev.2014.01.003.
397   (15)   Liang, S.; Hao, C.; Shi, Y. The Power of Single-Atom Catalysis. *ChemCatChem* **2015**,
398   *7* (17), 2559–2567. https://doi.org/10.1002/cctc.201500363.
399   (16)   Elmas, S.; Beelders, W.; Bradley, S. J.; Kroon, R.; Laufersky, G.; Andersson, M.;
400   Nann, T. Platinum Terpyridine Metallopolymer Electrode as Cost-Effective
401   Replacement for Bulk Platinum Catalysts in Oxygen Reduction Reaction and
402   Hydrogen Evolution Reaction. *ACS Sustainable Chemistry & Engineering* **2017**, *5*
403   (11), 10206–10214. https://doi.org/10.1021/acssuschemeng.7b02198.
404   (17)   Pu, Z.; Amiinu, I. S.; Cheng, R.; Wang, P.; Zhang, C.; Mu, S.; Zhao, W.; Su, F.; Zhang,
405   G.; Liao, S.; Sun, S. Single-Atom Catalysts for Electrochemical Hydrogen Evolution
406   Reaction: Recent Advances and Future Perspectives. *Nano-Micro Lett.* **2020**, *12*
407   (1), 21. https://doi.org/10.1007/s40820-019-0349-y.
408   (18)   Cheng, N.; Zhang, L.; Doyle-Davis, K.; Sun, X. Single-Atom Catalysts: From Design to
409   Application. *Electrochem. Energ. Rev.* **2019**, *2* (4), 539–573.
410   https://doi.org/10.1007/s41918-019-00050-6.

411   (19)   Piernavieja-Hermida, M.; Lu, Z.; White, A.; Low, K.-B.; Wu, T.; Elam, J. W.; Wu, Z.;
412   Lei, Y. Towards ALD Thin Film Stabilized Single-Atom Pd $_1$ Catalysts. *Nanoscale*
413   **2016**, *8* (33), 15348–15356. https://doi.org/10.1039/C6NR04403D.

414   (20)   Sun, S.; Zhang, G.; Gauquelin, N.; Chen, N.; Zhou, J.; Yang, S.; Chen, W.; Meng, X.;
415   Geng, D.; Banis, M. N.; Li, R.; Ye, S.; Knights, S.; Botton, G. A.; Sham, T.-K.; Sun, X.
416   Single-Atom Catalysis Using Pt/Graphene Achieved through Atomic Layer
417   Deposition. *Sci Rep* **2013**, *3* (1), 1775. https://doi.org/10.1038/srep01775.

418   (21)   Zhang, L.; Han, L.; Liu, H.; Liu, X.; Luo, J. Potential-Cycling Synthesis of Single
419   Platinum Atoms for Efficient Hydrogen Evolution in Neutral Media. *Angew. Chem.*
420   *Int. Ed.* **2017**, *56* (44), 13694–13698. https://doi.org/10.1002/anie.201706921.

421   (22)   Tavakkoli, M.; Holmberg, N.; Kronberg, R.; Jiang, H.; Sainio, J.; Kauppinen, E. I.;
422   Kallio, T.; Laasonen, K. Electrochemical Activation of Single-Walled Carbon
423   Nanotubes with Pseudo-Atomic-Scale Platinum for the Hydrogen Evolution
424   Reaction. *ACS Catal.* **2017**, *7* (5), 3121–3130.
425   https://doi.org/10.1021/acscatal.7b00199.

426   (23)   Zhang, J.; Zhao, Y.; Guo, X.; Chen, C.; Dong, C.-L.; Liu, R.-S.; Han, C.-P.; Li, Y.; Gogotsi,
427   Y.; Wang, G. Single Platinum Atoms Immobilized on an MXene as an Efficient
428   Catalyst for the Hydrogen Evolution Reaction. *Nat Catal* **2018**, *1* (12), 985–992.
429   https://doi.org/10.1038/s41929-018-0195-1.

430   (24)   Chen, Y.; Ji, S.; Chen, C.; Peng, Q.; Wang, D.; Li, Y. Single-Atom Catalysts: Synthetic
431   Strategies and Electrochemical Applications. *Joule* **2018**, *2* (7), 1242–1264.
432   https://doi.org/10.1016/j.joule.2018.06.019.

433   (25)   Gautier, C.; López, I.; Breton, T. A Post-Functionalization Toolbox for Diazonium
434   (Electro)-Grafted Surfaces: Review of the Coupling Methods. *Mater. Adv.* **2021**, *2*
435   (9), 2773–2810. https://doi.org/10.1039/D1MA00077B.

436   (26)   Bangle, R.; Sampaio, R. N.; Troian-Gautier, L.; Meyer, G. J. Surface Grafting of Ru(II)
437   Diazonium-Based Sensitizers on Metal Oxides Enhances Alkaline Stability for
438   Solar Energy Conversion. *ACS Appl. Mater. Interfaces* **2018**, *10* (3), 3121–3132.
439   https://doi.org/10.1021/acsami.7b16641.

440   (27)   Ghasemi, E.; Alimardani, E.; Shams, E.; Koohmareh, G. A. Modification of Glassy
441   Carbon Electrode with Iron-Terpyridine Complex and Iron-Terpyridine Complex
442   Covalently Bonded to Ordered Mesoporous Carbon Substrate: Preparation,
443   Electrochemistry and Application to H $_2$ O $_2$ Determination. *Journal of*
444   *Electroanalytical Chemistry* **2017**, *789*, 92–99.
445   https://doi.org/10.1016/j.jelechem.2017.01.043.

446   (28)   Albrecht, M.; van Koten, G. Platinum Group Organometallics Based on "Pincer"
447   Complexes: Sensors, Switches, and Catalysts. *Angewandte Chemie International*

448   *Edition* **2001**, *40* (20), 3750–3781. https://doi.org/10.1002/1521-
449   3773(20011015)40:20<3750::AID-ANIE3750>3.0.CO;2-6.

450 (29) Klein, A.; Elmas, S.; Butsch, K. Oxido Pincer Ligands - Exploring the Coordination
451   Chemistry of Bis(Hydroxymethyl)Pyridine Ligands for the Late Transition Metals.
452   *European Journal of Inorganic Chemistry* **2009**, *2009* (15), 2271–2281.
453   https://doi.org/10.1002/ejic.200900023.

454 (30) Klein, A.; Butsch, K.; Elmas, S.; Biewer, C.; Heift, D.; Nitsche, S.; Schlipf, I.;
455   Bertagnolli, H. Oxido-Pincer Complexes of Copper(II) – An EXAFS and EPR Study
456   of Mono- and Binuclear [(PydotH2)CuCl2]n (N=1 or 2). *Polyhedron* **2012**, *31* (1),
457   649–656. https://doi.org/10.1016/j.poly.2011.10.023.

458 (31) Chen, R.; Yang, C.; Cai, W.; Wang, H.-Y.; Miao, J.; Zhang, L.; Chen, S.; Liu, B. Use of
459   Platinum as the Counter Electrode to Study the Activity of Nonprecious Metal
460   Catalysts for the Hydrogen Evolution Reaction. *ACS Energy Lett.* **2017**, *2* (5),
461   1070–1075. https://doi.org/10.1021/acsenergylett.7b00219.

462 (32) Lee, J.; Bang, J. H. Reliable Counter Electrodes for the Hydrogen Evolution
463   Reaction in Acidic Media. *ACS Energy Lett.* **2020**, *5* (8), 2706–2710.
464   https://doi.org/10.1021/acsenergylett.0c01537.

465 (33) Gu, C.; Norris, B. C.; Fan, F.-R. F.; Bielawski, C. W.; Bard, A. J. Is Base-Inhibited
466   Vapor Phase Polymerized PEDOT an Electrocatalyst for the Hydrogen Evolution
467   Reaction? Exploring Substrate Effects, Including Pt Contaminated Au. *ACS*
468   *Catalysis* **2012**, *2* (5), 746–750. https://doi.org/10.1021/cs3000107.

469 (34) Tian, M.; Cousins, C.; Beauchemin, D.; Furuya, Y.; Ohma, A.; Jerkiewicz, G. Influence
470   of the Working and Counter Electrode Surface Area Ratios on the Dissolution of
471   Platinum under Electrochemical Conditions. *ACS Catal.* **2016**, *6* (8), 5108–5116.
472   https://doi.org/10.1021/acscatal.6b00200.

473 (35) Esposito, D. V. Membraneless Electrolyzers for Low-Cost Hydrogen Production in
474   a Renewable Energy Future. *Joule* **2017**, *1* (4), 651–658.
475   https://doi.org/10.1016/j.joule.2017.07.003.

476 (36) Winther-Jensen, B.; Fraser, K.; Ong, C.; Forsyth, M.; MacFarlane, D. R. Conducting
477   Polymer Composite Materials for Hydrogen Generation. *Advanced Materials* **2010**,
478   *22* (15), 1727–1730. https://doi.org/10.1002/adma.200902934.

479 (37) Gall, D. Electron Mean Free Path in Elemental Metals. *Journal of Applied Physics*
480   **2016**, *119* (8), 085101. https://doi.org/10.1063/1.4942216.

481 (38) Acres, R. G.; Ellis, A. V.; Alvino, J.; Lenahan, C. E.; Khodakov, D. A.; Metha, G. F.;
482   Andersson, G. G. Molecular Structure of 3-Aminopropyltriethoxysilane Layers
483   Formed on Silanol-Terminated Silicon Surfaces. *J. Phys. Chem. C* **2012**, *116* (10),
484   6289–6297. https://doi.org/10.1021/jp212056s.

485 (39) Elmas, S.; Macdonald, T.; Skinner, W.; Andersson, M.; Nann, T. Copper
486 Metallopolymer Catalyst for the Electrocatalytic Hydrogen Evolution Reaction
487 (HER). *Polymers* **2019**, *11* (1), 110. https://doi.org/10.3390/polym11010110.
488 (40) Cummings, S. D. Platinum Complexes of Terpyridine: Synthesis, Structure and
489 Reactivity. *Coordination Chemistry Reviews* **2009**, *253* (3–4), 449–478.
490 https://doi.org/10.1016/j.ccr.2008.04.013.
491 (41) Swiegers, G. F.; Malefetse, T. J. New Self-Assembled Structural Motifs in
492 Coordination Chemistry. *Chem. Rev.* **2000**, *100* (9), 3483–3538.
493 https://doi.org/10.1021/cr990110s.
494 (42) Hofmeier, H.; Schubert, U. S. Recent Developments in the Supramolecular
495 Chemistry of Terpyridine–Metal Complexes. *Chem. Soc. Rev.* **2004**, *33* (6), 373–
496 399. https://doi.org/10.1039/B400653B.
497 (43) Whittell, G. R.; Hager, M. D.; Schubert, U. S.; Manners, I. Functional Soft Materials
498 from Metallopolymers and Metallosupramolecular Polymers. *Nature Materials*
499 **2011**, *10* (3), 176–188. https://doi.org/10.1038/nmat2966.
500 (44) Dewi, M. R.; Gschneidtner, T. A.; Elmas, S.; Ranford, M.; Moth-Poulsen, K.; Nann, T.
501 Monofunctionalization and Dimerization of Nanoparticles Using Coordination
502 Chemistry. *ACS Nano* **2015**, *9* (2), 1434–1439.
503 https://doi.org/10.1021/nn5058408.
504 (45) Gao, Z.; Han, Y.; Gao, Z.; Wang, F. Multicomponent Assembled Systems Based on
505 Platinum(II) Terpyridine Complexes. *Acc. Chem. Res.* **2018**, *51* (11), 2719–2729.
506 https://doi.org/10.1021/acs.accounts.8b00340.
507 (46) Tian, J.; Liu, Q.; Asiri, A. M.; Sun, X. Self-Supported Nanoporous Cobalt Phosphide
508 Nanowire Arrays: An Efficient 3D Hydrogen-Evolving Cathode over the Wide
509 Range of PH 0–14. *J. Am. Chem. Soc.* **2014**, *136* (21), 7587–7590.
510 https://doi.org/10.1021/ja503372r.
511 (47) Sun, H.; Yan, Z.; Liu, F.; Xu, W.; Cheng, F.; Chen, J. Self-Supported Transition-Metal-
512 Based Electrocatalysts for Hydrogen and Oxygen Evolution. *Adv. Mater.* **2020**, *32*
513 (3), 1806326. https://doi.org/10.1002/adma.201806326.
514 (48) Tregubov, A. A.; Vuong, K. Q.; Luais, E.; Gooding, J. J.; Messerle, B. A. Rh(I)
515 Complexes Bearing *N* , *N* and *N* , *P* Ligands Anchored on Glassy Carbon Electrodes:
516 Toward Recyclable Hydroamination Catalysts. *J. Am. Chem. Soc.* **2013**, *135* (44),
517 16429–16437. https://doi.org/10.1021/ja405783g.
518 (49) Binding, S. C.; Pernik, I.; Gonçales, V. R.; Wong, C. M.; Webster, R. F.; Cheong, S.;
519 Tilley, R. D.; Garcia-Bennett, A. E.; Gooding, J. J.; Messerle, B. A. Simultaneous
520 Functionalization of Carbon Surfaces with Rhodium and Iridium Organometallic
521 Complexes: Hybrid Bimetallic Catalysts for Hydroamination. *Organometallics*
522 **2019**, *38* (4), 780–787. https://doi.org/10.1021/acs.organomet.8b00726.

523   (50) Pinson, J.; Podvorica, F. Attachment of Organic Layers to Conductive or
524   Semiconductive Surfaces by Reduction of Diazonium Salts. *Chem. Soc. Rev.* **2005**,
525   *34* (5), 429. https://doi.org/10.1039/b406228k.

526   (51) Elmas, S.; Skipper, K.; Salehifar, N.; Jamieson, T.; Andersson, G. G.; Nydén, M.;
527   Leterme, S. C.; Andersson, M. R. Cyclic Copper Uptake and Release from Natural
528   Seawater—A Fully Sustainable Antifouling Technique to Prevent Marine Growth.
529   *Environ. Sci. Technol.* **2021**, *55* (1), 757–766.
530   https://doi.org/10.1021/acs.est.0c06231.

531   (52) Ji, J.; Zhang, Y.; Tang, L.; Liu, C.; Gao, X.; Sun, M.; Zheng, J.; Ling, M.; Liang, C.; Lin, Z.
532   Platinum Single-Atom and Cluster Anchored on Functionalized MWCNTs with
533   Ultrahigh Mass Efficiency for Electrocatalytic Hydrogen Evolution. *Nano Energy*
534   **2019**, *63*, 103849. https://doi.org/10.1016/j.nanoen.2019.06.045.

535   (53) Xu, J.; Zhang, C.; Liu, H.; Sun, J.; Xie, R.; Qiu, Y.; Lü, F.; Liu, Y.; Zhuo, L.; Liu, X.; Luo, J.
536   Amorphous MoOX-Stabilized Single Platinum Atoms with Ultrahigh Mass Activity
537   for Acidic Hydrogen Evolution. *Nano Energy* **2020**, *70*, 104529.
538   https://doi.org/10.1016/j.nanoen.2020.104529.

539   (54) Yin, X.-P.; Wang, H.-J.; Tang, S.-F.; Lu, X.-L.; Shu, M.; Si, R.; Lu, T.-B. Engineering the
540   Coordination Environment of Single-Atom Platinum Anchored on Graphdiyne for
541   Optimizing Electrocatalytic Hydrogen Evolution. *Angew. Chem. Int. Ed.* **2018**, *57*
542   (30), 9382–9386. https://doi.org/10.1002/anie.201804817.

543   (55) Ghanim, A. H.; Koonce, J. G.; Hasa, B.; Rassoolkhani, A. M.; Cheng, W.; Peate, D. W.;
544   Lee, J.; Mubeen, S. Low-Loading of Pt Nanoparticles on 3D Carbon Foam Support
545   for Highly Active and Stable Hydrogen Production. *Front. Chem.* **2018**, *6*, 523.
546   https://doi.org/10.3389/fchem.2018.00523.

547   (56) Murto, P.; Elmas, S.; Méndez-Romero, U. A.; Yin, Y.; Genene, Z.; Mone, M.;
548   Andersson, G. G.; Andersson, M. R.; Wang, E. Highly Stable Indacenodithieno[3,2- *b*
549   ]Thiophene-Based Donor–Acceptor Copolymers for Hybrid Electrochromic and
550   Energy Storage Applications. *Macromolecules* **2020**, *53* (24), 11106–11119.
551   https://doi.org/10.1021/acs.macromol.0c02212.

552   (57) Kunwar, D.; Zhou, S.; DeLaRiva, A.; Peterson, E. J.; Xiong, H.; Pereira-Hernández, X.
553   I.; Purdy, S. C.; ter Veen, R.; Brongersma, H. H.; Miller, J. T.; Hashiguchi, H.; Kovarik,
554   L.; Lin, S.; Guo, H.; Wang, Y.; Datye, A. K. Stabilizing High Metal Loadings of
555   Thermally Stable Platinum Single Atoms on an Industrial Catalyst Support. *ACS*
556   *Catal.* **2019**, *9* (5), 3978–3990. https://doi.org/10.1021/acscatal.8b04885.

557   (58) Wagner, C. D. Chemical Shifts of Auger Lines, and the Auger Parameter. *Faraday*
558   *Discuss. Chem. Soc.* **1975**, *60*, 291. https://doi.org/10.1039/dc9756000291.

559   (59) Zagoraiou, E.; Daletou, M. K.; Sygellou, L.; Ballomenou, S.; Neophytides, S. G. Highly
560   Dispersed Platinum Supported Catalysts – Effect of Properties on the

561   Electrocatalytic Activity. *Applied Catalysis B: Environmental* **2019**, *259*, 118050.
562   https://doi.org/10.1016/j.apcatb.2019.118050.
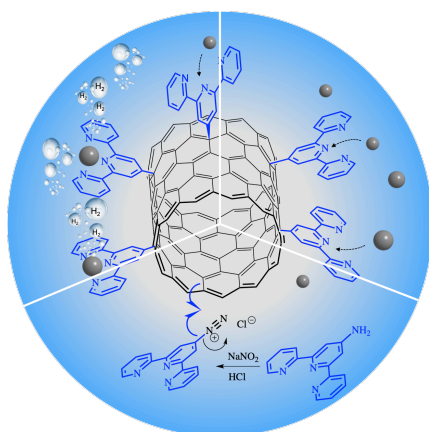
563

564

565

566 **TOC FIGURE**

567

568
569

570

571

"Highly Active Platinum Single-Atom Catalyst grafted onto 3D Carbon Cloth Support for the Electrocatalytic Hydrogen Evolution Reaction"

Po-Wei Yu[1], Sait Elmas[1]*, Xun Pan[1], Yanting Yin[1], Christopher T. Gibson[1,2], Gunther Andersson[1] and Mats R. Andersson[1]*

[1] - *Flinders Institute for Nanoscale Science & Technology, Flinders University, Bedford Park SA, Adelaide, Australia.*

2 - *Flinders Microscopy and Microanalysis, College of Science and Engineering, Flinders University, Bedford Park, SA 5042, Australia*

AUTHOR'S ORCID:

Sait Elmas: 0000-0002-1235-1436

Mats R. Andersson: 0000-0002-7928-8216

Gunther G. Andersson: 0000-0001-5742-3037

Xun Pan: 0000-0001-6087-7363

Christopher T. Gibson: 0000-0003-3334-5059

Calculating the value of Pt used in platinum single-atom catalysts on 3D carbon cloth electrode:

- Pt share price per ounce on 05.07.2021: 1107.1 US\$/ounce, which is 35.59 US\$/g.

- Catalyst loading in PtSAC@CC-0.5: 0.26 μg•cm^{-2} = $2.6 \cdot 10^{-7}$ g•cm^{-2}

- Pt loading in PtSAC@CC-0.5 on one square meter carbon cloth: $2.6 \cdot 10^{-3}$ g•m^{-2}

- Pt price on one square meter carbon cloth: $2.6 \cdot 10^{-3}$ g•m^{-2} * 35.59 US\$/g = **0.10 US\$•m^{-2}**

- For 20% 0.03 mg•cm^{-2} Pt/C the Pt loading is: $6 \cdot 10^{-6}$ g•cm^{-2}, which amounts to **2.13 US\$•m^{-2}**
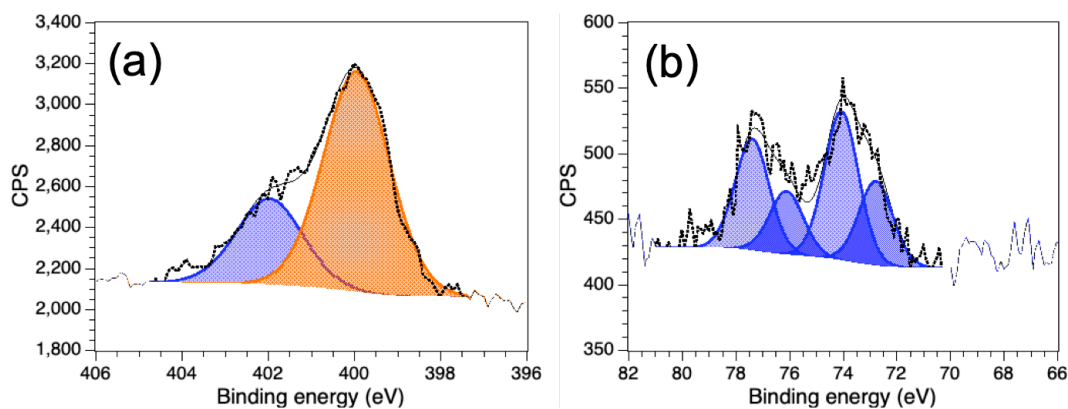
Figure S 1: Fitted (a) N1s and (b) Pt4f core level spectra of PtSAC-0.5 after 3 h chronoamperometric hydrogen evolution reaction at 10 mA•cm^{-2} in 0.5 M H$_2$SO$_4$ using a graphite rod as counter electrode.
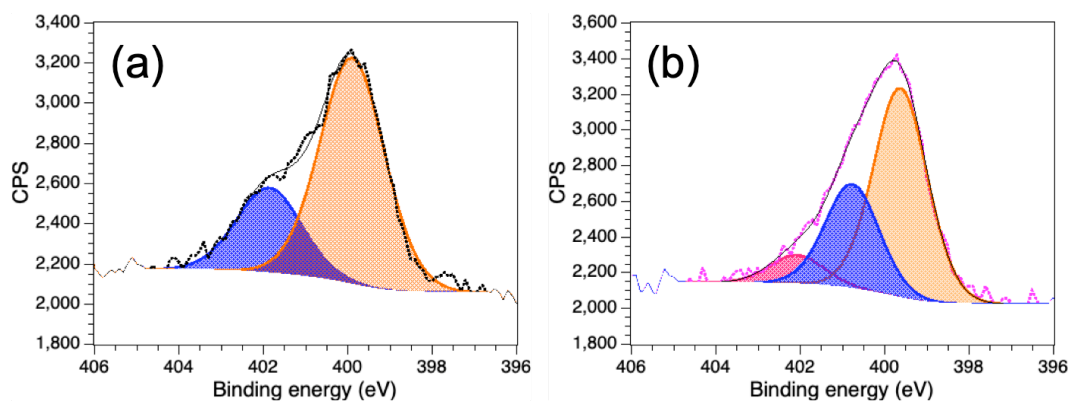
Figure S 2: Fitted N1s core level spectra of PtSAC-0.5 after 8 h chronoamperometric hydrogen evolution reaction at 10 mA•cm^{-2} in 0.5 M H$_2$SO$_4$ using a Pt wire as counter electrode before (a) and after (b) sonication for 4 minutes.